CrystEngComm

Accepted Manuscript

ROYAL SOCIETY OF CHEMISTRY

www.rsc.org/crystengcomm

Cite this: DOI: 10.1039/c0xx00000x

www.rsc.org/xxxxxx

PAPER

Facile synthesis of TiO_2 hollow spheres composed of high percentage reactive facets for enhanced photocatalytic activity

Bin Wang*[a,c1] Xiao-Ying Lu*[b1], Lawrence K. Yu[c,d], Jin Xuan[e], Michael K.H. Leung *[a] and Hongfan Guo[f]

Received (in XXX, XXX) Xth XXXXXXXXX 20XX, Accepted Xth XXXXXXXXX 20XX

DOI: 10.1039/b000000x

In this study, facile synthesis of TiO_2 hollow spheres composed of high percentage reactive facets (~85%) is successfully prepared with $TiOSO_4$ and HBF_4 by hydrothermal method. Results reveal that TiO_2 hollow spheres of 605 nm to 1.21 μm are anatase phase with sulfur doping. The variation of shell morphologies (*e.g.* polyhedral and nanosheet) can be realized by adjusting the reactant concentrations, while the molar ratio of $TiOSO_4$ to HBF_4 is maintained at 5:3. Based on the time-dependent morphology evolution study, the growth mechanism of hollow structure formation *via* self-templating and dissolution-recrystallization processes is discussed. Effects of reactant concentrations on TiO_2 morpholgy are investigated to understand the dual roles of HBF_4. Results also indicate that TiO_2 hollow spheres with nanosheet morphology having 85% percentage of (001) facets exhibit 1.4~5 times higher performance than their counterparts in photocatalytic hydrogen production. The enhanced photocatalytic activity is ascribed to the combined effects from unique hollow structure, high BET specific surface area (139.1 m^2/g) and high percentage of exposed reactive facets (85%). This study demonstrates a promising strategy for large-scale production of TiO_2 hollow spheres with template- and surfactant-free process for photocatalysis applications.

1 Introduction

Semiconductor photocatalysts have attracted significant attention due to their promising applications in converting solar energy into chemical energy and removing organic pollutants from water[1-6]. Among many photocatalysts, titanium dioxide (TiO_2) has received considerable interest due to its superior photocatalytic activity, chemical stability, low cost and nontoxicity[7, 8]. The photocatalytic performance can be significantly influenced by the morphology and microstructure of TiO_2. So far TiO_2 materials of different morphologies and nanostructures, such as nanowire[9, 10], nanotube[11-13] and nanosheet[14-16], have been developed for enhanced photocatalytic activity.

Recently, the use of TiO_2 hollow spheres has received much attention in the fields of catalysis, microreactor, adsorption and drug delivery, due to their low density, high surface area, good surface permeability and large light harvesting efficiency[17-20]. Many techniques have been developed for the fabrication of TiO_2 hollow spheres using removal or sacrificial templates. Kondo et .al reported that anatase TiO_2 hollow spheres were prepared by polystyrene (PS) bead as hard templates, followed by the removal of polystyrene beads by calcination [21]. Ao et al reported nitrogen-doped titania hollow spheres were successfully prepared by using carbon spheres as hard templates [22]. Besides, soft templates, such as surfactants, were also previously reported in the preparation of hollow TiO_2 spheres. Ding et.al used amino acid as multifunctional smart template to prepare mesoporous hollow TiO_2 spheres *via* solvothermal method [23]. In addition, Pan et al prepared hierarchical nitrogen-doped TiO_2 hollow spheres with nanothorns by a solvothermal method[24]. They found that the presence of diethylenethiamine played dual roles in the formation of nanothorns and nitrogen dopants. Although hard or soft templates have been successfully applied to TiO_2 hollow spheres synthesis, the typical disadvantages of using templates in material synthesis include high cost, tedious procedures and structure collapse on the removal of templates by calcinations or dissolution [25].

Template- and surfactant-free synthesis of hollow spheres is of great interest. Recently, Liu et al proposed a solvothermal method to prepare hollow TiO_2 microspheres with diameter of 1-2 μm, using $Ti(SO_4)_2$, NH_4F and ethanol as raw materials[26]. Ethanol was suggested as the stabilization reagent for TiO_2 polyhedra exposed with *ca.* 20% (001) facets. Li et.al also introduced a template-free approach to prepare hollow TiO_2 sphere using hydrolysis of $TiOSO_4$ in organic solvents (e.g. glycerol, alcohol and ethyl ether)[27]. Correspondingly, the use of organic solvents in material synthesis will increase the product cost and environmental burden. In addition, Yang et.al reported one pot approach to prepared hollow TiO_2 spheres *via* Ostwald ripening by hydrolysis of TiF_4 (1.33-2.67 mM) using hydrothermal method[28]. Although no soft or hard templates were directly required in their synthesis, the use of organic solvents and low concentration of TiO_2 precursor are the main obstacles for large-scale production. Therefore, it is desirable to develop a facile, economical and effective method to fabricate hollow TiO_2 spheres with controllable morphology and

size. In particular, TiO_2 hollow spheres composed of nanosheets with high percentage reactive (001) facets are highly desirable for practical applications, due to the enhanced photocatalytic activity in the utilization of solar energy[25].

In this study, a facile approach was proposed to prepare TiO_2 hollow spheres with (001) reactive facets as high as 85%. The formation mechanism of hollow structures was based on fluoride-mediated self-transformation strategy[25,29,30]. $TiOSO_4$ was used as TiO_2 precursor and sulfur source, and HBF_4 was employed as the fluoride precursor. The starting materials are simple and cheap without the addition of any organic structure directing agents and hard templates. The activities of the as-prepared hollow TiO_2 spheres were investigated by photocatalytic hydrogen production under UV-vis irradiation. Results suggest TiO_2 hollow spheres with nanosheet morphology having high percentage of (001) facets (*ca.* 85%) exhibit 1.4~5 times higher activity than their counterparts (TiO_2 nanoparticles and Degussa P25). Therefore, this method is facile and efficient in large-scale production of TiO_2 hollow spheres for practical photocatalysis applications.

2 Experimental section

2.1 Synthesis of TiO_2 hollow spheres

TiO_2 hollow spheres were prepared by a facile hydrothermal method with two chemicals, namely $TiOSO_4$ and HBF_4. In a typical synthesis, 0.2 g $TiOSO_4$ (technical grade, Sigma Aldrich), 0.125 mL HBF_4 (48wt.%, Sigma Aldrich) and 30 mL H_2O (Millipore, Inc.,18 $M\Omega \cdot cm^{-1}$) were added into a dry 50 mL Teflon-lined stainless steel autoclave. The concentration of $TiOSO_4$ was equivalent to 42 mM. The hydrothermal reaction was carried out at 180°C for 24 hours. After the reaction was completed, the autoclave was naturally cooled down to room temperature. The precipitation was harvested by centrifuge and sequentially washed with H_2O and ethanol for three times. Finally, the white product was dried at 60°C for 12 hours before material characterizations and photocatalytic activity test. This sample was denoted as TiO_2-HS-1. For comparison, a series of hollow TiO_2 spheres were synthesized with $TiOSO_4$ concentrations of 83 mM, 167 mM and 250 mM (TiO_2-HS-2: 0.4 g $TiOSO_4$ + 0.25 mL HBF_4 + 30 mL H_2O; TiO_2-HS-3: 0.8 g $TiOSO_4$ + 0.5 mL HBF_4 + 30 mL H_2O; TiO_2-HS-4: 1.2 g $TiOSO_4$ + 0. 75 mL HBF_4 + 30 mL H_2O). In addition, samples of TiO_2 hollow spheres (TiO_2-HS-1) for morphology evolution study were collected at different reaction stages (1h, 2h, 3h, 4h, 6h and 12h). TiO_2 sample synthesized without HBF_4 was also prepared as a control sample.

2.2 Material characterizations

Morphology and crystal structure analysis of the as-prepared TiO_2 materials were performed on field emission scanning electron microscope (FE-SEM, Hitachi S4800) and transmission electron microscope (TEM, FEI Tecnai G^2 20 scanning) equipped with selected area electron diffraction (SAED). The particle size and phase structure of TiO_2 hollow sphere powder samples were analyzed by X-ray diffractometer (XRD, Bruker) equipped with Cu $K_{\alpha 12}$ X-ray radiation and a LynxEye detector. The scanning range of 2θ was 10~80º with a step size of 0.02º and a scan speed of 0.2s/step. Oxidation state measurement of TiO_2 hollow sphere sample was measured on X-ray photoelectron spectroscopy (XPS, Model PHI5600). All binding energy was referenced to the C1s peak at 284.6 eV. Data processing was performed on software XPSPEAK 4.1. The optical properties of TiO_2 samples were recorded on diffuse reflectance UV–vis spectroscopy (DRS, UV-3010, Hitachi). N_2 adsorption-desorption isotherms of TiO_2 samples were conducted on surface area analyzer (Quantachrome Instruments) at liquid nitrogen temperature 77 K.

2.3 Photocatalytic hydrogen production

Photocatalytic hydrogen production over TiO_2 samples was performed in a closed gas circulation system (LabSolar, Trusttech, China) at room temperature. In a typical run, 40 mg as-prepared TiO_2 photocatalyst was ultrasonically dispersed in 100 mL 10 vol.% methanol solution (99.8%, Sigma Aldrich) followed by adding 1 mL platinum(II) acetylacetonate (99.99%, Sigma Aldrich) of 1 mg/mL, equivalent to 1.0 wt.% Pt loading. The photocatalyst suspension was then bubbled with N_2 gas for 60 min. Afterwards, a 300 W Xe lamp (Aulight, CEL-HX UV300, 200 nm - 2000 nm) was used to initiate the photo-reduction of Pt. Full spectrum light from 300 W Xe lamp with light intensity of about 100 mW/cm^2 was delivered from the top of the quartz cell for hydrogen production. The hydrogen production system was first evacuated by a vacuum pump and electromagnetic air pump was used to accelerate the gas circulation in the system. The gas sample in the system was periodically analyzed by a gas chromatograph (GC-2010, Shimadzu) equipped with Msieve 5A column (Restek, 30 m × 0.53 mm × 50 μm) and a thermal conductivity detector (TCD). The temperatures of inlet, column and detector were 35°C, 35°C and 120°C, respectively. Helium gas was used as the carrier gas at a flow rate of 30 mL/min.

3 Results and Discussion

3.1 Morphology analysis

Fig.1 shows FE-SEM images of the as-prepared TiO_2 samples under different reactant concentrations. As seen from Fig.1 (a)-(c), the sphere sizes of TiO_2-HS-1, TiO_2-HS-2 and TiO_2-HS-3 are found to be 605±11 nm, 1.21±0.04μm and 636±18 nm, respectively. Interestingly, the as-prepared TiO_2 spheres are also aggregated and form big clusters. The sphere sizes of TiO_2 in this work are smaller than previous studies, which reported hollow TiO_2 spheres were 1~8 μm in size [26, 31, 32]. However, when the concentration of $TiOSO_4$ is increased to 250 mM, only TiO_2 solid particles of ~100 nm in size are obtained, as seen in Fig. 1(d). This means that there is an optimum concentration range for the successful synthesis of TiO_2 hollow materials using $TiOSO_4$ and HBF_4. It should be noted that the TiO_2 precursor concentrations for hollow sphere fabrication in this work is about 30~125 times higher than previous work, suggesting the great potentials in large scale production of TiO_2 [27].

Fig.2 displays enlarged FE-SEM images of as-prepared TiO_2 hollow spheres. The hollow nature of as-prepared TiO_2 is evident from Fig. 2(a). In addition, a closer look at the morphologies in Fig. 2(b) indicates that the shell of TiO_2-HS-1 is composed of many ultrathin nanosheets. Constructing hollow spheres from building blocks of TiO_2 nanosheets with exposed reactive facets is considered as a great challenge[33]. According to previous work on TiO_2 nanosheets prepared by fluorides, the two flat and square surfaces were considered as the reactive (001) facets[34-36]. To further verify the exposed (001) facets, TEM and single crystal

electron diffraction pattern analysis of TiO_2 nanosheets are performed and shown in Fig. S1. (ESI†). The nanosheet morphology of TiO_2 in Fig. S1 is consisted with FE-SEM analysis (Fig. 2b). Also, the corresponding electron diffraction pattern of TiO_2 nanosheets indicated the (200) and (220) facets with *d*-spacing of 1.89 Å and 1.34 Å, respectively. Thus, zone axis is determined to be (001), demonstrating that TiO_2 nanosheets is exposed (001) facets. Yang et.al reported that F^- exhibited strong interaction with TiO_2 (001) facets and kinetically retarded the growth along (001) direction, leading to the nanosheet morphology[34].

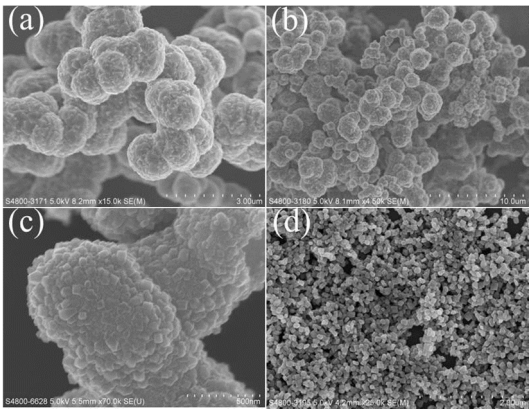

Fig. 1 FE-SEM images of the as-prepared TiO_2 samples with different concentrations (a) TiO_2-HS-1; (b) TiO_2-HS-2; (c) TiO_2-HS-3; (d) TiO_2-HS-4

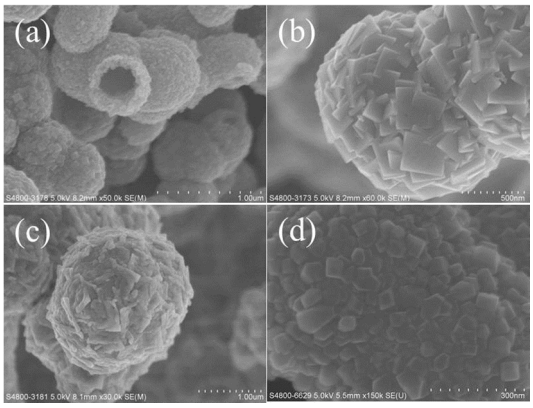

Fig. 2 Enlarged FE-SEM images of TiO_2 hollow spheres. (a) and (b) TiO_2-HS-1; (c) TiO_2-HS-2; (d) TiO_2-HS-3

The dimension of TiO_2 nanosheets in this work is estimated to be 340×340 nm and 30 nm in thick. The percentage of (001) reactive facets in TiO_2-HS-1 can be estimated by the following equation[37]:

$$\eta = \frac{2 \times A^2}{2 \times A^2 + 4 \times A \times H} \qquad (1)$$

where η is the percentage of (001) facets, A is the side length of nanosheet in nm and H is the thickness of nanosheet in nm. It is found that the percentage of (001) facets in TiO_2-HS-1 is 85%, which is much higher than previous work. Liu et. al reported 1~2 μm TiO_2 hollow spheres composed of anatase polyhedral having *ca.* 20% (001) facets[26]. However, with the increase of $TiOSO_4$ concentration, the shell morphology of TiO_2-HS-2 in Fig. 2(c) is consisted of irregular coarse surface. Fig. 2(d) suggests that many polyhedral TiO_2 with an estimated size of ~40 nm are formed on the external surface of TiO_2-HS-3. The shell morphology should be ascribed to the increased reactant concentrations, which can significantly affect the reaction rates of dissolution and recrystallization. The unique shell structures of TiO_2 hollow spheres are quite different from the conventional TiO_2 sphere with smooth surface and can greatly influence their photocatalytic activity[30].

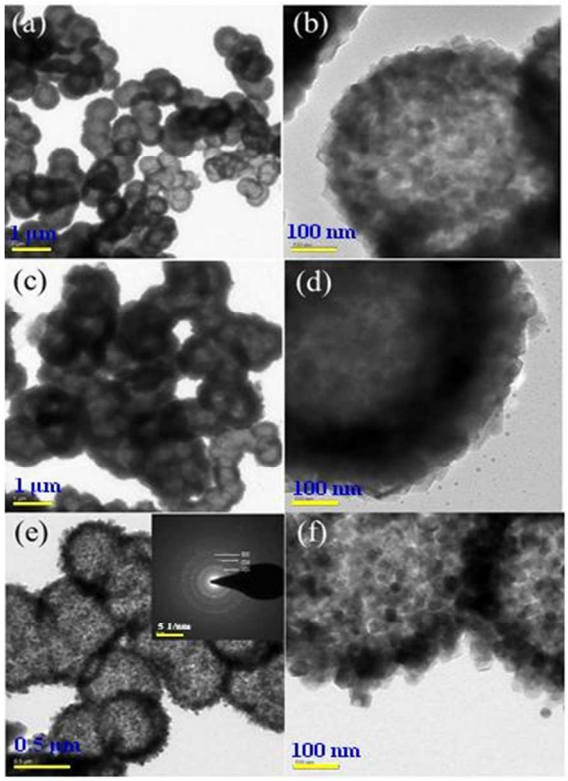

Fig. 3 TEM images of the as-prepared TiO_2 hollow spheres (a) and (b): TiO_2-HS-1; (c) and (d): TiO_2-HS-2; (e) and (f): TiO_2-HS-3; The inset is the selected area electron diffraction (SAED) pattern

The uniform hollow structure of TiO_2-HS-1, TiO_2-HS-2 and TiO_2-HS-3 is further confirmed by TEM images, as shown in Fig. 3(a)-(f). It is suggested that controllable synthesis of TiO_2 hollow spheres can be successfully achieved by hydrolysis of $TiOSO_4$ with concentrations, ranging from 42 mM to 167 mM, while the molar ratio of $TiOSO_4$ to HBF_4 is maintained at 5:3. Jiang et. al reported the control of sphere size and structure (multi-hollow or single-hollow) by varying the concentration of starting materials[38]. In addition, the porous nature can be clearly observed in these hollow spheres, indicated by the obvious contrast (dark and bright) in the TEM images. The inset SAED image in Fig.3(e) confirms high crystallization degree of the as-prepared TiO_2 sample. The *d*-spacing of 3.5 Å, 2.4 Å and 1.9 Å correspond to the anatase TiO_2 crystal facets (101), (004) and (200), respectively.

To understand the roles of HBF_4 in the formation of TiO_2 hollow spheres with reactive facets, pure TiO_2 sample is also synthesized only with 0.8 g $TiOSO_4$ and 30 mL H_2O. Fig. 4 presents FE-SEM images of TiO_2 synthesized without HBF_4 for 1 hour and 24 hours. As shown in Fig. 4(a) and (b), only solid TiO_2 spheres of around 3.8 μm are obtained for 1 hour hydrothermal

reaction. However, for 24 hour reaction, the particle size of TiO_2 solid sphere with distorted shell is about 900 nm, suggesting that TiO_2 spheres are partially dissolved with the increase of reaction time. The control experiment implies that the formation of hollow spheres is probably due to the self-templating process. HBF_4 plays critical roles in the formation and self-assembly of TiO_2 nanosheets as well as creating interior cavity by dissolution-recrystallization process. More detailed discussion will be given in the morphology evolution and growth mechanism of TiO_2 hollow spheres.

3.2 Crystal phase analysis

The phase structure of the as-prepared TiO_2 hollow spheres was investigated by XRD technique and the result is shown in Fig.5. It can be seen that major 2θ peaks at 25.3°, 37.8° and 48.0° match the characteristic peaks of the anatase TiO_2 (PDF card No: 21-1272; tetragonal; space group: $I4_1/amd$ (141)), in good agreement with electron diffraction pattern (Fig. 3e). The average crystalline size of the as-prepared TiO_2 sample can be determined by Debye-Scherer formula, based on the main anatase diffraction (101) peak [39].

$$D = K\lambda/\beta \cos\theta \qquad (2)$$

where D is the crystalline size, λ the wavelength of X-ray radiation (0.1541 nm), K the constant usually taken as 0.89 and β is the peak width (in radians) at half-maximum height. The crystal size of TiO_2 is calculated to be 32~46 nm, in good agreement with the TEM observations. Hence, TiO_2 of pure anatase phase can be successfully prepared by hydrothermal approach using $TiOSO_4$ and HBF_4.

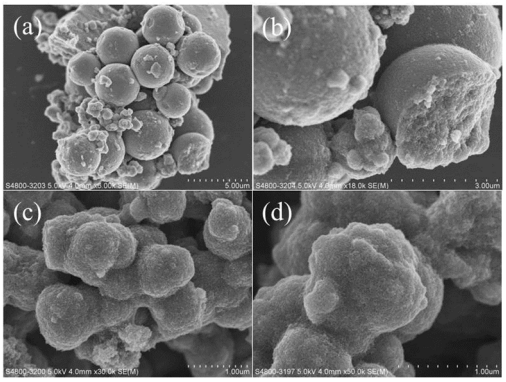

Fig. 4 FE-SEM images of TiO_2 synthesized with 0.8 g $TiOSO_4$ and 30 mL H_2O for different durations (a) and (b): 1 hour; (c) and (d): 24 hours

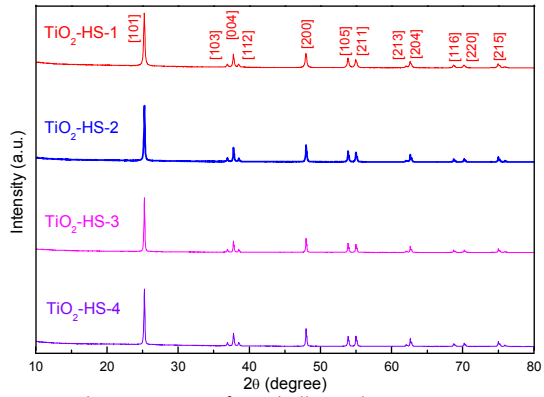

Fig. 5 Typical XRD patterns of TiO_2 hollow spheres

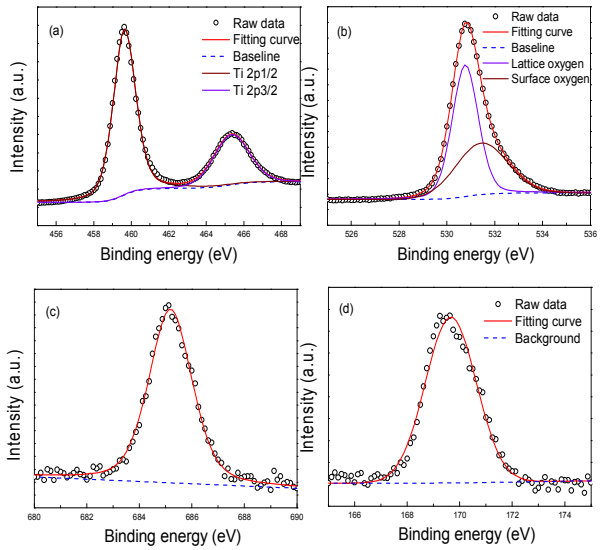

Fig. 6 High resolution XPS spectra of TiO_2-HS-1 hollow spheres (a) Ti2p; (b) O1s; (c) F1s; (d) S2p

3.3 XPS analysis

Fig. 6 depicts typical high resolution XPS spectra of the as-prepared TiO_2-HS-1 hollow spheres. The survey spectrum in Fig. S2 (ESI†) suggests that the TiO_2 sample contains Ti, O, F, S and C. It should be mentioned that the C element is mainly ascribed to the hydrocarbon from XPS itself [20]. The binding energy values for Ti2p3/2 (B.E. =459.7 eV) and Ti2p1/2 (B.E. = 465.4 eV) shown in Fig. 6(a) confirm that the titanium is of oxidation state +4 [40, 41]. The XPS spectrum for O1s in Fig. 6(b) can be deconvoluted into two peaks. This indicates that oxygen is present as O^{2-} in TiO_2 lattice (B.E. =530.8 eV) and surface oxygen in the form of M-OH (B.E. =531.5 eV, M=Ti and/or S). Surface oxygen plays important roles in enhancing photocatalytic activity. It is suggested that hydroxyl group can capture the photogenerated holes, forming highly reactive hydroxyl free radicals[42]. The effective inhabitation of electron-hole recombination can improve the photocatalytic activity of TiO_2. Fig. 6(c) shows XPS spectrum for F1s region. The binding energy of F1s is 685.2 eV, suggesting the presence of ≡Ti-F species on the TiO_2 crystal surface[43].

Fig. 6(d) shows the high resolution XPS spectrum of S2p region. It is found that S atoms are in the state S^{6+} in the TiO_2 sample with a binding energy of 169.7eV, consistent with previous work[44]. This peak suggested S species are in the form of SO_4^{2-} by substituting Ti atoms in the lattice of TiO_2 [45]. It should be mentioned that peak at around 162 eV (B.E. of Ti-S) is not detected. This confirms that S atoms are not likely to substitute O atoms in TiO_2. The ionic radius of S^{6+}, Ti^{4+}, S^{2-} and O^{2-} are 43, 74.5, 170 and 126 pm, respectively[46]. The reason for the favorable substitution of Ti^{4+} by S^{6+} is that the ionic radii difference between S^{6+} and Ti^{4+} is smaller than that between S^{2-} and O^{2-}. Moreover, composition analysis by XPS indicates that the atomic concentrations of Ti, S and O are 27.73%, 1.23% and 58.38%, respectively. The atomic ratio of Ti, S to O is 0.95:0.04:2, further suggesting the substitution of Ti with S. The replacement of Ti^{4+} by S^{6+} can lead to the imbalanced charge, which can probably be neutralized by the hydroxide ions [44].

It should be noted that the ionic form of S is dependent on the

synthesis methods and the starting materials used. Previously, Naik et. al reported that S was doped in TiO_2 in the cationic form (S^{6+}) when titanium oxysulfate sulfuric acid complex and thiourea were used as TiO_2 precursor and dopant sources[47], in good agreement with this work. However, Umebayashi et.al reported S dopant was in the anionic form (S^{2-}) when TiS_2 was used as the raw material with oxidation annealing method [48].

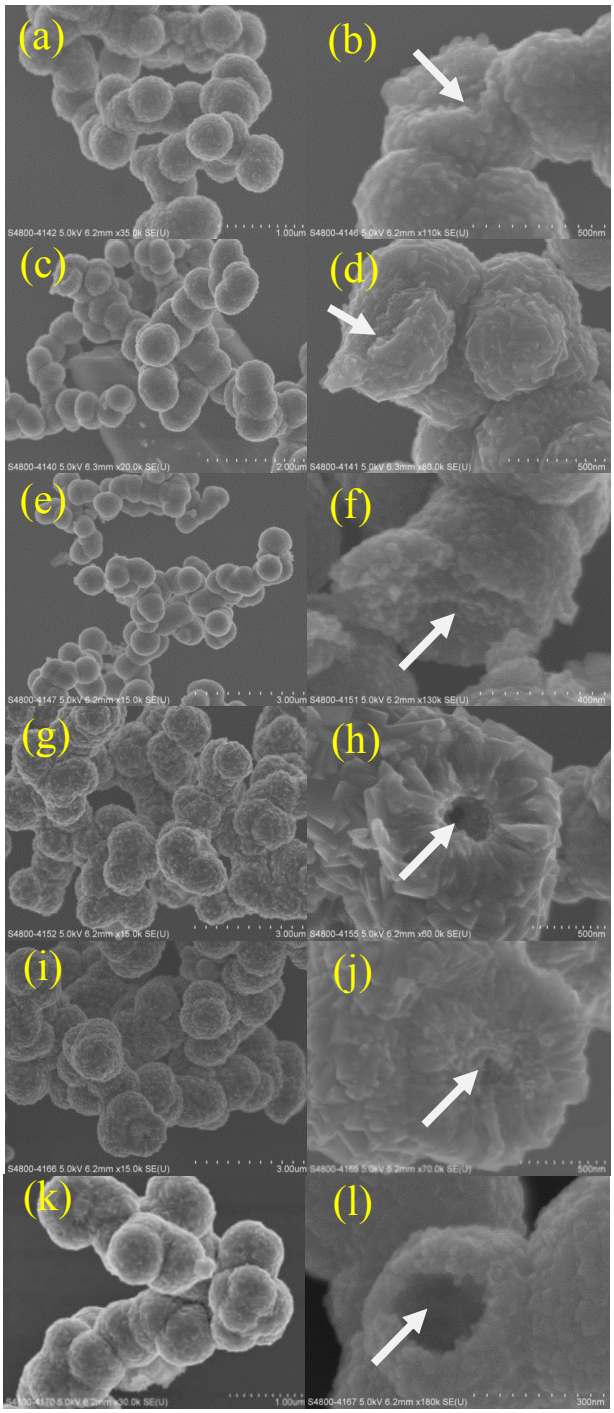

Fig. 7 FE-SEM images of morphology evolution of TiO_2-HS-1 hollow spheres synthesized with 0.2 g $TiOSO_4$ + 0.125 mL HBF_4 + 30 mL H_2O. (a) and (b): 1 hour; (c) and (d): 2 hours; (e) and (f): 3 hours; (g) and (h): 4 hours; (i) and (j): 6 hours; (k) and (l): 12 hours. Arrow: the core of TiO_2 spheres. (a)-(f): solid spheres; (g)-(l): hollow spheres

3.4 Morphology evolution

Fig. 7 shows FE-SEM images of TiO_2-HS-1 samples collected at different hydrothermal stages. TiO_2 sphere size estimated from FE-SEM images as a function of reaction time is plotted in Fig. S3 (ESI†). XRD analysis of TiO_2-HS-1 samples collected at different stages is also presented in Fig.S4 (ESI†). The time-dependent changes in morphology, crystal phase and size are informative to understand the growth mechanism of TiO_2 hollow structure. As seen in Fig. 7(a) and (b), TiO_2 solid sphere of 869±22 nm is obtained for reaction duration of 1 hour. This sphere size is much smaller than that obtained without HBF_4 (*ca.* 3.8 μm), which indicates the presence of HBF_4 can effectively inhibit the growth of TiO_2. Also, well-defined shell can be found on the surface of TiO_2 solid spheres. XRD peaks of TiO_2-HS-1 at this stage are broad and crystal phase can be as assigned to anatase (PDF card No: 21-1272), indicating the formation of small crystallite size. At reaction duration of 2 hours, as shown in Fig.7(c) and (d), solid sphere size of 558±19 nm is obtained. The size reduction implies the dissolution of TiO_2 spheres occurs at the first 2 hours, possibly due to the etching of small sized TiO_2 by HBF_4. When hydrothermal reaction lasts for 3 hours, the solid sphere size is determined to be 681±16 nm, as seen in Fig.7(e) and (f). The size increase of solid spheres implies that shell growth of TiO_2 happens on the surface of spheres. With the increase of reaction time to 4 hours, the sphere size is estimated to be 939±42 nm. Interestingly, obvious hollow structures start to appear from inside-out, witnessed by Fig.7 (g) and (h). The shell thickness and cavity diameter are around 365 nm and 313 nm, respectively. Also, sheet morphology began to form through recrystallization process. In Fig.7(i) and (j), TiO_2 spheres of 1.05±0.06 μm with sharp edges can be clearly found. The wall thickness and cavity diameter are approximately 218 nm and 573 nm, respectively. From Fig.7(j), tiny TiO_2 particles can be apparently observed in the cavity of the product and are considered as the weak sites for the invasion by fluorides. Previous work suggested that TiO_2 nanoparticles having large surface to volume ratio and high surface energy tend to grow into larger spheres, due to the minimization of the total interfacial energy[30]. The size changes in wall thickness and cavity diameter further confirms the inside-out ripening mechanism. When the reaction time is 12 hours, as shown in Fig.7(k) and (l), The sphere size is around 878±39 nm. The well-crystalline nanosheet morphology and hollow structure can be obviously observed. This size is slightly larger than the product obtained at 24 hours (*ca.* 605±11 nm). This indicates further ripening process could occur in the later hydrothermal process. The time-dependent XRD analysis also suggests that TiO_2 of anatase phase forms immediately by fast hydrolysis of $TiOSO_4$. The crystallite sizes at different stages (e.g. 2~12 h) estimated by XRD analysis are almost the same, implying dissolution-recrystallization process in hydrothermal reactions. To further understand morphology evolution, TiO_2-HS-2 samples collected at different stages are also investigated by FE-SEM. Similarly, as shown in Fig. S5 (ESI†), solid spheres can be observed at the very beginning (e.g. 1 h) and obvious hollow structure starts to form at an earlier stage (e.g. 2 h), compared to TiO_2-HS-1 (e.g. 4 h). This should be due to the relatively high reactant concentrations, which can accelerate the process of dissolution-recrystallization under

hydrothermal conditions. Notably, as shown in Fig. S5(g) (ESI†), TiO_2 hollow spheres with nanosheet morphology are observed at a reaction time of 4 h and further increasing of reaction time can change nanosheets into cubic-shaped structures. It should also be mentioned that the formation mechanism of hollow spheres in this work is different with previous study, which reported that the presence of core-shell and sphere-in-shell intermediate product in the early reaction stage[49].

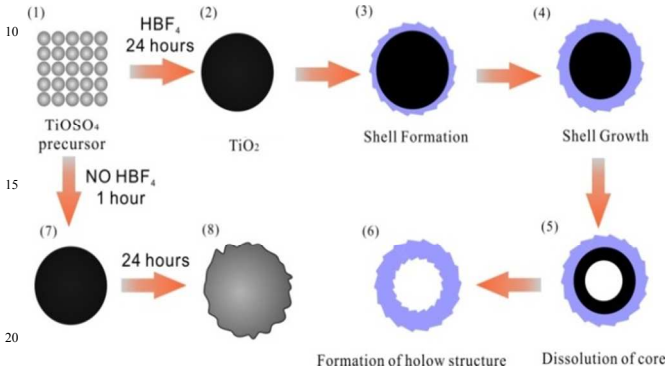

Fig. 8 Schematic illustration of formation of hollow structure

3.5 Proposed formation mechanism of TiO_2 hollow spheres

Fig. 8 illustrates the formation mechanism of hollow TiO_2-HS-1 and TiO_2-HS-2 spheres, based on experimental findings, fluoride-mediated self-transformation and Ostwald ripening theory[25,49,50]. The formation of TiO_2 hollow spheres is first initiated by fast hydrolysis of $TiOSO_4$, which can be completed within 1 h. The involved hydrolysis reactions are proposed in reaction (3) and (4). As confirmed by XRD and FE-SEM, solid spheres composed of small sized TiO_2 function as the hard templates for the subsequent growth of well-defined hollow structure *via* self-templating process. Also, well-defined structures of TiO_2 (e.g. nanosheets and polyhedral) and small pores are formed on the outer surface. The presence of pores is beneficial for the invasion of TiO_2 cores by fluorides (F^-) released from the decomposition of HBF_4. Previous study implied that F^- can be used in favor of producing anatase TiO_2 with reactive facts[42]. Therefore, the unique shell structures (polyhedral and nanosheet) are due to the presence of fluorides as morphological directing agents. The TiO_2 shell in anatase phase is relatively stable due to the protection by ≡Ti-F bonds, as indicated by XPS. On the contrary, the small sized TiO_2 with porous structure is not stable under hydrothermal conditions and can be gradually etched by the fluoride ions in the strong acidic medium. The reaction between small sized TiO_2 and F^- ions is described in previous studies [51], as shown in reaction (5).

$$TiOSO_4 + 2H_2O \rightarrow TiO(OH)_2 \quad (3)$$

$$TiO(OH)_2 \rightarrow TiO_2\,(\text{small crystalline}) + H_2O \quad (4)$$

$$TiO_2\,(\text{small crystalline}) + 6F^- + 4H^+ \rightarrow TiF_6^{2-} + 2H_2O \quad (5)$$

$$TiF_6^{2-} + 4H_2O \rightarrow Ti(OH)_4 + 4HF + 2F^- \quad (6)$$

$$Ti(OH)_4 \rightarrow TiO_2\,(\text{anatase shell}) + 2H_2O \quad (7)$$

At the same time, the as-formed TiF_6^{2-} species can be reused in the construction of TiO_2 hollow spheres, according to the reaction (6) and (7)[52]. After the complete dissolution of TiO_2 core, hollow TiO_2 spheres with stable anatase polyhedral and nanosheet structures are formed. Therefore, TiO_2 hollow spheres can be successfully prepared *via* self-templating and dissolution-recrystallization processes without the participation of any structure directing surfactants or hard templates.

In this work, localized Ostwald ripening or fluoride-mediated self-transformation is believed to be the driving force for the formation of TiO_2 hollow spheres with well-defined shells. The shell morphologies are sensitive to reactant concentrations in the hydrothermal process. This is because reactant concentrations have significant impacts on the reaction rates of TiO_2 dissolution and recrystallization. In the hydrothermal synthesis, the molar ratio of $TiOSO_4$ to HBF_4 is mainly kept at 5:3. This molar ratio can control the balance between dissolution rate and recrystallization rate. When the reactant concentration ($TiOSO_4$= 42 mM) is low, the recrystallization process should have higher reaction rate than dissolution rate, due to the lower concentration of F^-. Thus, well-defined nanosheets with high percentage reactive facets can be formed in the shell. When the reactant concentration is increased ($TiOSO_4$ = 83~167 mM), only disordered or polyhedral structures can be found in the shell layers. With further increase of $TiOSO_4$ concentration to 250 mM, only small nanoparticles are found in the final product, suggesting that TiO_2 dissolution rate is higher than TiO_2 recrystallization. The accelerated dissolution rate is likely due to the higher concentration of F^- in the hydrothermal reaction, thus leading to the collapse of TiO_2 shell by finally forming small nanoparticles. Based on this strategy, Huang et.al recently reported the conversion from $TiOF_2$ nanocubes to anatase TiO_2 nanoboxes composed with (001) facets *via* inside-outside dissolution-recrystallization process[53].

3.6 Effects of reactant concentrations on TiO_2 morphologies

In this study, TiO_2 hollow spheres with different shell morphologies can be successfully synthesized by keeping the molar ratio of $TiOSO_4$ to HBF_4 at 5:3. In order to further understand the effects of HBF_4 and $TiOSO_4$ concentrations on TiO_2 morphologies, the molar ratio of reactants is adjusted in the range of 5:1.5 to 5:18. As shown in Fig. S6 (ESI†) , when the amount of added $TiOSO_4$ is maintained at 0.2 g and the volume of added HBF_4 is increased from 0.0625 mL to 0.75 ml, significant effects of HBF_4 concentration on TiO_2 formation are found. No TiO_2 product is formed when the HBF_4 volume is increased to 0.5 mL and 0.75 mL, probably due to the etching effect of F^- released from the decomposition of HBF_4 at hydrothermal conditions. Also, the TiO_2 morphology synthesized at molar ratio of 5:1.5 and 5:6 are quite different with 5:3 (TiO_2-HS-1). As shown in Fig. S7 (ESI†), when the added HBF_4 is 0.0625 mL or 0.25 mL, hollow structure of TiO_2 is not obvious at low HBF_4 concentration and no nanosheets can be found on the TiO_2 surface at high HBF_4 concentration. It should be mentioned that the obvious dissolution of TiO_2 begins at HBF_4 volume of 0.25 mL, indicated by the relatively smooth surface. Thus, dual roles of HBF_4 in controlling the morphology of TiO_2 are suggested. On one hand, F^- released from HBF_4 can stabilize the (001) facets and inhibit the growth of growth along (001) direction. On the other hand, F^- can also react with TiO_2 to form soluble species (e.g. TiF_6^{2-}) by etching process. To further confirm the dual effects of HBF_4, the volume of added HBF_4 is fixed at 0.125 ml and the molar ratio of $TiOSO_4$ to HBF_4 is tuned

in the range of 2.5:3 to 20:3. Similarly, as shown in Fig.S8 (ESI†), no TiO_2 nanosheet morphology or hollow structure can be observed with excess or insufficient HBF_4. Thus, synthesis of TiO_2 hollow spheres with nanosheet structure is sensitive to the reactant concentrations and reactant molar ratios.

3.7 Photocatalytic hydrogen production

Fig.9 exhibits photocatalytic hydrogen production over the as-prepared TiO_2 hollow spheres with different shell morphologies. The hydrogen production performance of Degussa P25 and TiO_2 nanoparticles (TiO_2-HS-4) synthesized with 1.2 g $TiOSO_4$ are also studied as a reference. Based on the 4-hour measurement, hydrogen production rate of TiO_2-HS-1, TiO_2-HS-2, TiO_2-HS-3, TiO_2-HS-4 and Degussa P25 are determined to be 299, 100, 144, 57 and 215 μmol/h/g , respectively. Obviously, TiO_2-HS-1 with hollow structure and 85% reactive (001) facets shows the best hydrogen evolution performance, compared to other TiO_2 samples (e.g. nanoparticles and Degussa P25). Hydrogen production rate of TiO_2-HS-1 is 5 times higher than that of TiO_2 nanoparticles, 3 times higher activity than TiO_2-HS-2 and 2 times higher than TiO_2-HS-3. Previous work suggested four crucially important factors involved in photocatalysis process, namely, the structure of the photocatalyst, the adsorption of reactants, the light absorption and the electron-hole transportation and separation[54]. Thus, UV-*vis* diffuse reflectance spectra and N_2 adsorption-desorption isotherms of TiO_2 samples are also compared and discussed to explain the enhancement of photocatalytic activity.

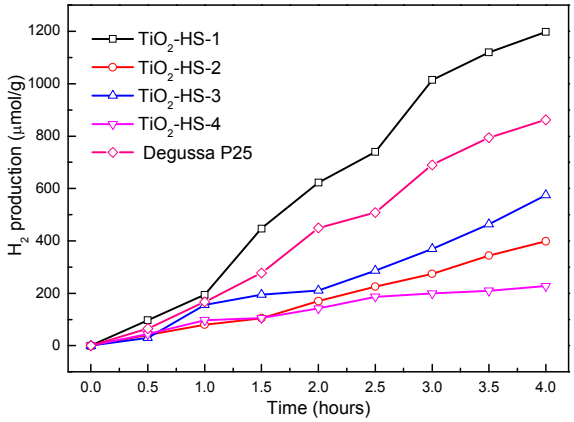

Fig. 9 Photocatalytic hydrogen production over the as-prepared TiO_2 samples

According to UV-*vis* diffuse reflectance spectra (DRS) in Fig. S9 (ESI†), the band gaps of TiO_2-HS-1, TiO_2-HS-2 and TiO_2-HS-3 are almost the same and determined to be in the range of 3.0~3.1 eV. Also, the band gap of Degussa P25 is calculated to be 3.1 eV, consistent with previous work[55]. Thus, the band gaps of TiO_2 show no significant effect on their photocatalytic H_2 production performance. DRS measurement can also provide useful information of light-scattering ability of the microstructures. Ferber et.al reported computer simulation of light-scattering in TiO_2 electrode of dye-sensitized solar cells and found that TiO_2 particles (250~300 nm) could be used as effective light scatterers to improve solar absorption[56]. In addition, Bao et.al reported that high light-scattering ability could effectively extend the optical path in TiO_2 microstructures, thus improving the light harvesting efficiency and achieving better photocatalytic performance[57]. Recently, Qian et. al also found multilayered hollow spherical structure could enhance light-harvesting efficiency. They suggested the shells of different sizes in a microsphere could also scatter the incident light of different wavelengths in the range of visible light[58].

As shown in Fig. S10 (ESI†), N_2 adsorption-desorption isotherms of TiO_2 samples (TiO_2-HS-1, TiO_2-HS-2 and TiO_2-HS-3) exhibit typical type-IV isotherms and type H3 hysteresis loops, indicating the presence of mesopores, in good agreement with TEM analysis (Fig. 3). The specific BET surface areas of TiO_2-HS-1, TiO_2-HS-2, TiO_2-HS-3 and P25 are 139.1 m^2/g, 80.4 m^2/g, 78.1 m^2/g and 56.2 m^2/g. The significant difference in specific surface area is probably due to the different microstructures of TiO_2. The highest specific surface area of TiO_2-HS-1 is mainly attributed to the ultrathin nanosheet structures as the building units of hollow TiO_2 spheres. The specific surface area of P25 is close to the value reported in literature[59]. The high specific surface area is beneficial for the adsorption of reactant (e.g. methanol and water) involved in photocatalysis. In addition, as mentioned, the nanostructures of TiO_2 photocatalysts and photogenerated electron-hole transportation and separation are important factors in photocatalysis.

Based on FE-SEM and TEM analysis, TiO_2-HS-1 is hollow sphere structure. Previous work implied that hollow structure was beneficial for the enhancement of photocatalytic activity. Truong et.al reported TiO_2 hollow spheres of 2 μm showed higher hydrogen production performance than TiO_2 nanoparticles[60]. Zhou et.al also found hollow TiO_2 micro/nanostructures templated from bacteria showed 3.6 times higher activity than the solid counterpart in hydrogen production[61]. As suggested by Li et. al, the high activity of TiO_2 hollow spheres is also due to the multireflections of light inside the interior cavities, endowing the unique hollow structure with enhanced photocatalytic hydrogen production activity[27]. It should be mentioned that the hydrogen production rate of TiO_2-HS-1 is not as high as bacteria-templated hollow TiO_2 spheres (577.7~625.5μmol/h/g)[61]. The difference should be due to the different photocatalytic test conditions, such as stronger light irradiance (e.g. 400 mW/cm^2) etc [61].

More importantly, TiO_2-HS-1 shows 3 times higher activity than TiO_2-HS-2 and 2 times higher than TiO_2-HS-3, even though all of them are endowed with hollow structure. Except for the high specific surface area, high percentage of exposed reactive (001) facets in TiO_2-HS-1 also plays critical roles in photocatalysis. The surface free energy of the (001) facets (0.90 J/m^2) is approximately 1.4 times higher than that of thermodynamically more stable (101) facets[62]. Previous work suggested the dominant (001) high-energy facets exhibited substantial effects on the dissociative adsorption of reactant molecules and effective separation of photo-excited electrons and holes, thus improving the photocatalytic activity[63]. The interaction between water molecules and TiO_2 surface was previously investigated and the chemically dissociated water molecules are energetically favored on the (001) facets[64]. In addition, charge separation can be also promoted by (001) facets, avoiding the recombination of electrons and holes. Recent study mentioned the unique atomic geometries, surface defects and

surface energies of (001) could affect the surface electronic structures, giving rise to a possible divergent diffusion of photo-generated electrons and holes toward different exposed facets[65]. Recently, Tachikawa et. al found the directional flow of photogenerated charge carriers toward specific facets using single-molecule, single-particle fluorescence approach[66]. In a word, unique hollow structure, high specific surface area and high percentage of reactive facets of TiO_2-HS-1 are the major reasons for the enhanced photocatalytic activity.

It should be mentioned that commercially available Degussa P25 (TiO_2 nanoparticles) also shows good photocatalytic water splitting performance in comparison with TiO_2-HS-2 and TiO_2-HS-3. Although P25 exhibits the close band gap and slightly low specific surface area, the crystal phase of P25 is quite different from the as-prepared TiO_2-HS-2 and TiO_2-HS-3 (e.g. anatase). It is found that the coexistence of anatase and rutile phases is observed in P25, as indicated by XRD analysis in Fig. S11 (ESI†). Previous study also reported that P25 with a particle size of ~25 nm was consists of 70% anatase phase and 30% rutile phase [67,68]. Thus, the improved photocatalytic activity compared with pure anatase powders is due to the effective electron and hole transfer between these two phases[69].

Tuning shell morphology of TiO_2 hollow spheres is of significant importance for improving TiO_2 photocatalytic activity. Up to now, most previous studies focused on the making of hollow structure and adjusting the sphere size, ignoring the tuning of surface morphology [60,61,70]. Previous work suggested that nanostructured TiO_2 with high percentage of (001) facets generally showed higher photocatalytic activity[34, 35]. Yu et. al reported TiO_2 nanosheets with (001) reactive facets exhibited much higher photocatalytic hydrogen production activity than Degussa P25 TiO_2 and pure TiO_2 nanoparticles[71]. However, recycling of nanosized photocatalysts is more difficult and challenging, as compared to submicron-sized hollow spheres. It should be mentioned that quantum efficiency of TiO_2 in phtocatalytic hydrogen generation was generally low and not investigated in this study. Qi et.al reported CdS sensitized Pt/TiO_2 composites can achieve quantum efficiency of 13.9% at 420 nm[72]. Therefore, further modification of TiO_2 hollow spheres composed of high percentage reactive facets is required in the future work. In a word, to the best of our knowledge, it is the first time to report template- and surfactant-free synthesis of TiO_2 hollow spheres composed with nanosheet shell having 85% reactive (001) facets and high BET specific surface area (139.1 m^2/g), demonstrating great potentials in photocatalysis and lithium ion battery applications.

4 Conclusions

In conclusion, facile synthesis of TiO_2 hollow spheres endowed with 85% (001) reactive facets is successfully achieved for the first time by hydrothermal method using $TiOSO_4$ and HBF_4. The shell morphology and sphere size of TiO_2 hollow spheres can be tuned by adjusting the reactant concentrations. It is also found that HBF_4 plays critical roles in the formation and self-assembly of TiO_2 nanosheets as well as creating interior cavity. The formation of hollow structure follows the self-templating and dissolution-recrystallization processes. Photocatalytic hydrogen production study implies that TiO_2 hollow spheres with nanosheet morphology exhibits 1.4~5 times higher performance than their counterparts, due to the unique hollow structure, high BET specific surface area and high percentage (001) reactive facets. This template- and surfactant-free strategy has potential applications in the large-scale production of nanostructured TiO_2 hollow spheres.

Acknowledgements

The research works presented in this paper are funded by the Ability R&D Energy Research Centre and CityU Project 7200297. Financial supports from Technological and Higher Education Institute of Hong Kong Seed Grant Scheme (No: 1415103) and Hong Kong Innovation and Technology Fund (No: ITF/162/12FX) are acknowledged. Mr. Surya Avinash Avala is also gratefully acknowledged for his help in photocatalytic hydrogen production experiment.

Notes and references

[a] *Ability R&D Energy Research Centre, School of Energy and Environment, City University of Hong Kong, Hong Kong, China. E-mail: mkh.leung@cityu.edu.hk Fax: +852-34420688; Tel: +852-34424626*

[b] *Faculty of Science and Technology, Technological and Higher Education Institute of Hong Kong, Hong Kong, China. Email: xylu@vtc.edu.hk Fax: +852-21761554; Tel: +852-21761453*

[c] *Green Energy, Sensing & Integration Group, Hong Kong Applied Science and Technology Research Institute Company Limited, Hong Kong. Email: bwang@astri.org Fax: +852-34062802; Tel: +852-34062561*

[d] *Department of Chemical and Biological Engineering, Princeton University, Princeton, NJ 08544, USA*

[e] *Institute of Mechanical, Process and Energy Engineering, School of Engineering & Physical Sciences, Heriot-Watt University, Edinburgh EH14 4AS, United Kingdom*

[f] *College of Chemical Engineering, Shenyang University of Chemical Technology, Shenyang, China*

[1] *These authors are equally contributed to this article*

† Electronic Supplementary Information (ESI) available: [TEM image and single crystal electron diffraction pattern of TiO_2 nanosheets, XPS survey spectrum of TiO_2-HS-1 hollow spheres, the size growth of TiO_2 sphere as a function of reaction time, XRD patterns of TiO_2-HS-1 collected at different stages, FE-SEM images of TiO_2-HS-2 collected at different stages, digital photos of the as-prepared TiO_2 samples, FE-SEM images of TiO_2 samples synthesized with different molar ratios of $TiOSO_4$ to HBF_4, UV-*vis* diffuse reflectance spectra of TiO_2 samples; N_2 adsorption-desorption isotherms and specific surface areas of TiO_2 samples; XRD pattern of Degussa P25 sample]. See DOI: 10.1039/b000000x/

1 V. J. Babu, M. K. Kumar, A. S. Nair, T. L. Kheng, S. I. Allakhverdiev and S. Ramakrishna, *Int. J. Hydrogen. Energ.*, 2012, **37**, 8897-8904.

2 K. Iwashina and A. Kudo, *J. Am. Chem. Soc.*, 2011, **133**, 13272-13275.

3 K. Baransi, Y. Dubowski and I. Sabbah, *Water Res.*, 2012, **46**, 789-798.

4 H. Widiyandari, A. Purwanto, R. Balgis, T. Ogi and K. Okuyama, *Chem. Eng. J.*, 2012, **180**, 323-329.

5 M. Ni, M. K. H. Leung, D. Y. C. Leung and K. Sumathy, *Renew. Sust. Energ. Rev.*, 2007, **11**, 401-425.

6 C. H. Ao, M. K. H. Leung, R. C. W. Lam, D. Y. C. Leung, L. L. P. Vrijmoed, W. C. Yam and S. P. Ng, *Chem. Eng. J.*, 2007, **129**, 153-159.

7 J. Zhang, Q. Xu, Z. Feng, M. Li and C. Li, *Angew. Chem. Int. Edit.*, 2008, **47**, 1766-1769.
8 S. Liu, E. Guo and L. Yin, *J. Mater. Chem.*, 2012, **22**, 5031-5041
9 Q. Wang, Z. Wen and J. Li, *Adv. Funct. Mater.*, 2006, **16**, 2141-2146.
10 X. Feng, K. Shankar, O. K. Varghese, M. Paulose, T. J. Latempa and C. A. Grimes, *Nano Lett.*, 2008, **8**, 3781-3786.
11 S. P. Albu, A. Ghicov, J. M. Macak, R. Hahn and P. Schmuki, *Nano Lett.*, 2007, **7**, 1286-1289.
12 O. K. Varghese, M. Paulose and C. A. Grimes, *Nat. Nanotechnol.*, 2009, **4**, 592-597.
13 J. H. Park, S. Kim and A. J. Bard, *Nano Lett.*, 2006, **6**, 24-28.
14 S. Feng, J. Yang, H. Zhu, M. Liu, J. Zhang, J. Wu and J. Wan, *J. Am. Chem. Soc.*, 2011, **94**, 310-315.
15 Q. Xiang, J. Yu, W. Wang and M. Jaroniec, *Chem. Commun.*, 2011, **47**, 6906-6908.
16 J. Yu, L. Qi and M. Jaroniec, *J. Phys. Chem. C*, 2010, **114**, 13118-13125.
17 X. W. Lou, L. A. Archer and Z. C. Yang, *Adv. Mater.*, 2008, **20**, 3987-4019.
18 J. Q. Li, D. F. Wang, H. I. Liu, Z. L. He and Z. F. Zhu, *Appl. Surf. Sci.*, 2011, **257**, 5879-5884.
19 J. G. Yu, S. W. Liu and H. G. Yu, *J. Catal.*, 2007, **249**, 59-66.
20 J. J. Xu, M. D. Chen and D. G. Fu, *Appl. Surf. Sci.*, 2011, **257**, 7381-7386.
21 Y. Kondo, H. Yoshikawa, K. Awaga, M. Murayama, T. Mori, K. Sunada, S. Bandow and S. Iijima, *Langmuir*, 2008, **24**, 547-550.
22 Y. H. Ao, J. J. Xu, D. G. Fu and C. W. Yuan, *J. Hazard. Mater.*, 2009, **167**, 413-417.
23 S. J. Ding, F. Q. Huang, X. L. Mou, J. J. Wu and X. J. Lu, *J. Mater. Chem.*, 2011, **21**, 4888-4892.
24 J. H. Pan, G. Han, R. Zhou and X. S. Zhao, *Chem. Commun.*, 2011, **47**, 6942-6944.
25 J. G. Yu and J. Zhang, *Dalton Trans.*, 2010,**39**,5860-5867.
26 S. W. Liu, J. G. Yu and M. Jaroniec, *J. Am. Chem. Soc.*, 2010, **132**, 11914-11916.
27 H. X. Li, Z. F. Bian, J. Zhu, D. Q. Zhang, G. S. Li, Y. N. Huo, H. Li and Y. F. Lu, *J. Am. Chem. Soc.*, 2007, **129**, 8406-8407.
28 H. G. Yang and H. C. Zeng, *J. Phys. Chem. B*, 2004, **108**, 3492-3495.
29 J. G. Yu, H. T. Guo, S. A. Davis and S. Mann, *Adv. Funct. Mater.*, 2006, **16**, 2035-2041.
30 S. W. Liu, J. G. Yu and S. Mann, *Nanotechnology*, 2009, **20**. 325606–325613
31 X. Du, J. H. He and Y. Q. Zhao, *J. Phys. Chem. C*, 2009, **113**, 14151-14158.
32 J. G. Wang, Y. Yang, Z. H. Huang and F. Y. Kang, *J. Power Sources*, 2012, **204**, 236-243.
33 S. J. Ding, J. S. Chen, Z. Y. Wang, Y. L. Cheah, S. Madhavi, X. A. Hu and X. W. Lou, *J. Mater. Chem.*, 2011, **21**, 1677-1680.
34 H. G. Yang, C. H. Sun, S. Z. Qiao, J. Zou, G. Liu, S. C. Smith, H. M. Cheng and G. Q. Lu, *Nature*, 2008, **453**, 638-U634.
35 X. G. Han, Q. Kuang, M. S. Jin, Z. X. Xie and L. S. Zheng, *J. Am. Chem. Soc.*, 2009, **131**, 3152-3153.
36 F. Amano, O. O. Prieto-Mahaney, Y. Terada, T. Yasumoto, T. Shibayama and B. Ohtani, *Chem. Mater.*, 2009, **21**, 2601-2603.
37 B. Wang, M. K. H. Leung, X. Y. Lu and S. Y. Chen, *Appl. Energ.* 2013, **112**, 1190-1197.
38 J. Jiang, F. Gu, W. Shao and C. Z. Li, *Ind. Eng. Chem. Res.*, 2012, **51**, 2838-2845.
39 C. Wang, Y. H. Ao, P. F. Wang, J. Hou, J. Qian and S. H. Zhang, *J. Hazard. Mater.*, 2010, **178**, 517-521.
40 D. B. Hamal and K. J. Klabunde, *J. Phys. Chem. C*, 2011, **115**, 17359-17367.
41 Y. Cong, X. K. Li, Y. Qin, Z. J. Dong, G. M. Yuan, Z. W. Cui and X. J. Lai, *Appl. Catal. B-Environ.*, 2011, **107**, 128-134.
42 S. Q. Shang, X. L. Jiao and D. R. Chen, *ACS Appl. Mater. Inter.*, 2012, **4**, 860-865.
43 H. G. Yang, G. Liu, S. Z. Qiao, C. H. Sun, Y. G. Jin, S. C. Smith, J. Zou, H. M. Cheng and G. Q. Lu, *J. Am. Chem. Soc.*, 2009, **131**, 4078-4083.
44 J. C. Yu, W. K. Ho, J. G. Yu, H. Yip, P. K. Wong and J. C. Zhao, *Environ. Sci. Technol.*, 2005, **39**, 1175-1179.
45 Q. J. Xiang, J. G. Yu and M. Jaroniec, *Phys. Chem. Chem. Phys.*, 2011, **13**, 4853-4861.
46 R. D. Shannon, *Acta Crystallogr. A*, 1976, **32**, 751-767.
47 B. Naik, K. M. Parida and C. S. Gopinath, *J. Phys. Chem. C*, 2010, **114**, 19473-19482.
48 T. Umebayashi, T. Yamaki, H. Itoh and K. Asai, *Appl. Phys. Lett.*, 2002, **81**, 454-456.
49 K. L. Lv, B. Cheng, J. G. Yu and G. Liu, *Phys. Chem. Chem. Phys.*, 2012, 14, 5349-5362.
50 B. Liu and H. C. Zeng, *Small*, 2005, **1**, 566-571.
51 M. M. Lohrengel, *Mat. Sci. Eng. R*, 1993, **11**, 243-294.
52 Q. J. Xiang, J. G. Yu and M. Jaroniec, *Chem. Commun.*, 2011, **47**, 4532-4534.
53 Z.A. Huang, Z.Y. Wang, K. L. Lv, Y. Zheng and K. J. Deng, *ACS Appl. Mater. Inter.,* 2013, **5**, 8663-8669.
54 K. Dai, L. Lu, Q. Liu, G. Zhu, Q. Liu and Z. Liu, *Dalton Trans.*, 2014, **43**, 2202-2210.
55 F. Zheng, Z. Wang, J. Chen and S. Li, *RSC Adv.*, 2014, **4**, 30605-30609.
56 J. Ferber and J. Luther, *Sol. Energ. Mat. Sol. Cells*, 1998, **54**, 265-275.
57 Z. Q. Bao, H. Xie, Q. Zhu, J. Qian, P. Ruan and X. Zhou, *CrystEngComm*, 2013, **15**, 8972-8978.
58 J. Qian, P. Liu, Y. Xiao, Y. Jiang, Y. Cao, X. Ai and H. Yang, *Adv. Mater.*, 2009, **21**, 3663-3667.
59 M.-Y. Xing, B.-X. Yang, H. Yu, B.-Z. Tian, S. Bagwasi, J.-L. Zhang and X.-Q. Gong, *J. Phys. Chem. Lett.*, 2013, **4,** 3910-3917.
60 Q. D. Truong, T. S. Le and H. T. Hoa, *CrystEngComm*, 2012, **14**, 4274-4278.
61 H. Zhou, T. X. Fan, J. Ding, D. Zhang and Q. X. Guo, *Opt. Express*, 2012, **20**, A340-A350.
62 Y.-W. Jun, M. F. Casula, J.-H. Sim, S. Y. Kim, J. Cheon and A. P. Alivisatos, *J. Am. Chem. Soc.*, 2003, **125**, 15981-15985.
63 S. Liu, J. Yu and M. Jaroniec, *Chem. Mater.*, 2011, **23**, 4085-4093.
64 A. Selloni, *Nat Mater.*, 2008, **7**, 613-615.
65 N. Murakami, Y. Kurihara, T. Tsubota and T. Ohno, *J. Phys. Chem. C*, 2009, **113**, 3062-3069.
66 T. Tachikawa, S. Yamashita and T. Majima, *J. Am. Chem. Soc.*, 2011, **133**, 7197-7204.
67 H. R. Jafry, M. V. Liga, Q. Li and A. R. Barron, *Environ. Sci. Technol.*, 2010, **45**, 1563-1568.
68 Y. Tang, P. Wee, Y. Lai, X. Wang, D. Gong, P. D. Kanhere, T.-T. Lim, Z. Dong and Z. Chen, *J. Phys. Chem. C*, 2012, **116**, 2772-2780.
69 D. C. Hurum, A. G. Agrios, K. A. Gray, T. Rajh and M. C. Thurnauer, *J. Phys. Chem. B*, 2003, **107**, 4545-4549.
70 J. B. Joo, Q. Zhang, I. Lee, M. Dahl, F. Zaera and Y. D. Yin, *Adv. Funct. Mater.*, 2012, **22**, 166-174.
71 J. G. Yu, L. F. Qi and M. Jaroniec, *J. Phys. Chem. C*,2010, **114**, 13118-13125.
72 L. F. Qi, J. G. Yu and M. Jaroniec, *Phys. Chem. Chem. Phys*, 2011, **13**, 8915-8923.